Available online at www.sciencedirect.com
SCIENCE DIRECT®
Physica A 362 (2006) 93–97
PHYSICA A
www.elsevier.com/locate/physa

Modeling viscoelastic flow with discrete methods

Ellák Somfai*, Alexander N. Morozov, Wim van Saarloos

Instituut-Lorentz, Universiteit Leiden, PO Box 9506, 2300 RA Leiden, Netherlands

Available online 5 October 2005

Abstract

The hydrodynamics of viscoelastic materials (for example, polymer melts and solutions) presents interesting and complex phenomena, for example, instabilities and turbulent flow at very low Reynolds numbers due to normal stress effects and the existence of a finite stress relaxation time. This present work is motivated by renewed interest in instabilities in polymer flow. The majority of currently used numerical methods discretize a constitutive equation on a grid with finite difference or similar methods. We present work in progress in which we simulate viscoelastic flow with dissipative particle dynamics. The advantage of this approach is that many of the numerical instabilities of conventional methods can be avoided, and that the model gives clear physical insight into the origins of many viscoelastic flow instabilities.

Keywords: Dissipative particle dynamics; Viscoelastic fluids

1. Introduction

One of the most important properties of viscoelastic fluids is that shear flow affects not only the off-diagonal (shear) component of the stress tensor, but also the diagonal elements: they change with respect to each other [1,2]. In the plane Couette flow geometry of Fig. 1, where the viscosity η is

$$\sigma_{xz} = \eta\dot{\gamma} \tag{1}$$

($\sigma_{\alpha\beta}$ is the stress tensor and $\dot{\gamma} = \partial v_x/\partial z$ is the shear rate), the first normal stress difference N_1 is defined as

$$\sigma_{xx} - \sigma_{zz} = N_1(\dot{\gamma}) = \Psi_1\dot{\gamma}^2, \tag{2}$$

where the first normal stress coefficient Ψ_1 is finite for small shear rate $\dot{\gamma}$.

Many of the unusual flow phenomena of viscoelastic fluids can be traced back to this nonzero normal stress difference. The extra forces generated by the viscoelastic stresses often destabilize the flow, leading to instabilities. This work has been motivated by the realization that many key issues regarding viscoelastic instabilities are unresolved. For example, it was suggested recently that while the viscoelastic Poiseuille flow might be linearly stable, it could be nonlinearly unstable, and this might be a route to melt-fracture type behavior [3,4]. These viscoelastic instabilities occur even at vanishing Reynolds numbers, and are driven not by kinetic forces but by elastic forces. The control parameter is the Weissenberg number Wi, the ratio of the

*Corresponding author.
E-mail address: ellak@lorentz.leidenuniv.nl (E. Somfai).

0378-4371/$ - see front matter
doi:10.1016/j.physa.2005.09.025

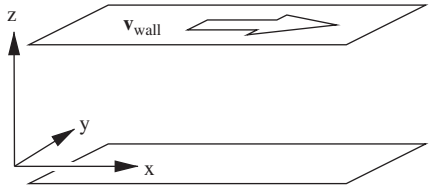

Fig. 1. The plane Couette flow geometry of our simulations.

characteristic relaxation time of the fluid (τ) and the characteristic time of the flow: for a shear flow it is $\dot{\gamma}\tau$. As Wi is increased, the instabilities lead to a complex nonstationary flow, often called viscoelastic turbulence [5,6], based on similarities to the Reynolds number driven turbulence.

Clearly numerical methods are in great need to understand these complex phenomena. However, the classical rheological engineering approach, based on finite volume or finite difference discretization of the Navier–Stokes equation together with the viscoelastic constitutive equations, runs into numerical instabilities in what is commonly referred to as "high Weissenberg number problem" [7]. Our goal is to overcome this barrier by turning to alternative, discrete methods of fluid dynamics.

In this paper we describe an extension of one of the successful discrete methods, the dissipative particle dynamics (DPD), to viscoelastic fluids. In this approach we do not start from a closed set of equations, instead use kinetic considerations. This work is in progress, and we show the first validation results.

2. Dissipative particle dynamics

In the method of DPD [8,9] the fluid is represented with particles, each one corresponding to a macroscopic blob of the fluid. The particles interact with each other via finite range pairwise forces. The force exerted on particle i of a Newtonian fluid can be written as a sum of conservative, dissipative and random contributions:

$$\mathbf{f}_i = \sum_{j \neq i} (\mathbf{f}_{ij}^{\text{cons}} + \mathbf{f}_{ij}^{\text{diss}} + \mathbf{f}_{ij}^{\text{rand}}). \tag{3}$$

The conservative part of the force is a soft repulsion:

$$\mathbf{f}_{ij}^{\text{cons}} = \begin{cases} a(1 - r_{ij}/r_{\text{c}})\hat{\mathbf{r}}_{ij}, & r_{ij} < r_{\text{c}}, \\ 0, & r_{ij} \geqslant r_{\text{c}}, \end{cases} \tag{4}$$

where $\mathbf{r}_{ij} = \mathbf{r}_i - \mathbf{r}_j$ is the separation vector of the particles, with distance $r_{ij} = |\mathbf{r}_{ij}|$, and unit vector $\hat{\mathbf{r}}_{ij} = \mathbf{r}_{ij}/r_{ij}$.

The dissipative part of the force acts to equalize velocities of nearby particles. It is also central force:

$$\mathbf{f}_{ij}^{\text{diss}} = -\gamma w^{\text{diss}}(r_{ij})(\hat{\mathbf{r}}_{ij} \cdot \mathbf{v}_{ij})\hat{\mathbf{r}}_{ij}. \tag{5}$$

The random part of the force represents a coupling to a heat bath:

$$\mathbf{f}_{ij}^{\text{rand}} = \sigma w^{\text{rand}}(r_{ij})\xi_{ij}\hat{\mathbf{r}}_{ij}, \tag{6}$$

where $\xi_{ij} = \xi_{ji}$ is a Gaussian random variable, independent for each ij pair of particles and timestep, with zero mean and Δt^{-1} variance.

The coefficients γ and σ and the two weight functions cannot be chosen arbitrarily: in order that the fluctuation-dissipation theorem holds [9], they must be related by

$$w^{\text{diss}}(r) = [w^{\text{rand}}(r)]^2, \tag{7}$$

$$\sigma^2 = 2\gamma k_{\text{B}} T. \tag{8}$$

We use the following weight function [10]:

$$w^{\mathrm{diss}}(r) = [w^{\mathrm{rand}}(r)]^2 = \begin{cases} \sqrt{1 - r/r_c}, & r < r_c, \\ 0, & r > r_c. \end{cases} \tag{9}$$

Given the interparticle forces, Newton's equations of motion are solved with a version of the velocity-Verlet algorithm [11]. As customary, our units were the cutoff length r_c and the mass of a particle.

In our plane Couette flow geometry (see Fig. 1) we have periodic boundary conditions in the x (streamwise) and y (spanwise) direction, and no-slip walls perpendicular to the z (gradient) axis. The walls are implemented as a soft repulsion potential in the normal direction:

$$\mathbf{f}_z^{\mathrm{wall}} = \begin{cases} -a^{\mathrm{wall}} z, & z < 0, \\ 0, & 0 \leqslant z \leqslant L \quad \text{(in bulk)}, \\ a^{\mathrm{wall}}(z - L), & z > L, \end{cases} \tag{10}$$

where L is the distance between the walls. To realize no-slip boundary conditions, at each timestep we update the particles' velocity component parallel to the walls as

$$\mathbf{v}_{\parallel} \quad \Leftarrow \quad \mathbf{v}_{\parallel} + \alpha(z)(\mathbf{v}^{\mathrm{wall}} - \mathbf{v}_{\parallel}), \tag{11}$$

where the factor $\alpha(z)$ is selected so that the velocity is unaffected in the bulk, the wall velocity is imposed upon particles well outside the walls, and there is a continuous crossover between these limits. Near the bottom wall it is

$$\alpha(z) = \begin{cases} 0, & z \geqslant 0 & \text{(in bulk)}, \\ -z/d_0, & -d_0 < z < 0 & \text{(near wall)}, \\ 1, & z \leqslant -d_0 & \text{(well outside wall)} \end{cases} \tag{12}$$

and similarly defined near the top wall. This approach is admittedly not elegant, as for example it has a nontrivial timestep dependence, but nevertheless achieves no-slip boundary conditions with minimal effort.

With these boundary conditions the particles wander outside the nominal wall position to a limited distance depending on the temperature and pressure. For too sharp walls the density near the walls displays oscillations as a function of distance from the wall. These are probably the consequence of local crystallization near a sharp surface. This unphysical phenomenon is avoided by softening the wall; we used $a^{\mathrm{wall}} = a$.

The z components of the stress tensor at the walls are readily available from the momentum transfer between the wall and the particles. In the bulk, however, they have to be computed from the pairwise forces [12]:

$$\sigma_{\alpha\beta} = \frac{1}{V}\left\{ -\sum_{\langle i,j \rangle} \mathbf{f}_{ij,\alpha} \mathbf{r}_{ij,\beta} - \sum_i m_i (\mathbf{v}_i - \bar{\mathbf{v}})_\alpha (\mathbf{v}_i - \bar{\mathbf{v}})_\beta \right\}. \tag{13}$$

We validated our code for Newtonian fluids by calculating the stresses with different methods: at the walls, the global bulk value (where $\bar{\mathbf{v}}$ is taken as the average velocity of particles at the same height z), and calculated locally [here Eq. (13) is integrated with a coarse graining kernel, which vanishes outside the neighborhood of a point]. All measurements were equal within error except the local stress, which differed by 10%—we attribute this to the difference in the contribution of fluctuations. We then calculated the viscosity from the shear stress, which compared well with an independent measurement from the relaxation time of the shear velocity profile's build-up at sudden start-up of the shear boundary conditions from rest.

3. DPD for viscoelastic fluids

To simulate viscoelastic hydrodynamics we connected DPD particles with springs: some fraction (in this paper all) of the particles are paired up to form dumbbells, so Eq. (3) receives an extra term $\mathbf{f}^{\mathrm{dumb}}$. Linear (Hookean) springs give rise to nonphysical effects in elongational flow [2], therefore we used finite extensible

nonlinear elastic (FENE) springs:

$$\mathbf{f}^{\mathrm{dumb}}(\mathbf{r}) = \frac{H\mathbf{r}}{1-(r/r_{\max})^2}, \tag{14}$$

where $\mathbf{r}$ is the separation between the endpoints of the dumbbell, H is the Hookean spring stiffness (at zero extension), and $r_{\max}$ is the maximum extension of the spring.

As the first validation test, we measured the velocity profile in our shear cell, and obtained the expected linear profile. The shear viscosity, however, is now weakly dependent on the shear rate, as shown in Fig. 2a.

We also measured the first normal stress difference, see Fig. 2b. The figure shows that the model does achieve its goal, namely that it yields a normal stress difference, which for small $\dot{\gamma}$ increases as $\dot{\gamma}^2$. At shear rate $\dot{\gamma} \gtrsim 1$, the coefficient Ψ_1 starts to decrease notably.

The viscoelastic modes are represented by the FENE dumbbells, to which we have full access in the numerical simulations. Fig. 3 shows the distribution of dumbbell orientation and extension. At low shear rates the dumbbells are isotropically oriented. At larger shear rates the dumbbells become elongated, with the typical orientation at a small angle with the stream direction. At the highest shear rate the distribution shows almost zero angle of the dumbbells with respect to the stream lines.

The time evolution of a typical dumbbell orientation is plotted in Fig. 4. For small shear rates the trajectory resembles a random walk in the configuration space, while at larger shear rates the dumbbells tumble: if by fluctuation the two endpoints get to different height z, they are dragged with different velocities, resulting in a horizontal stretch. If at this point the endpoints move to the same height, the differential drag disappears, and

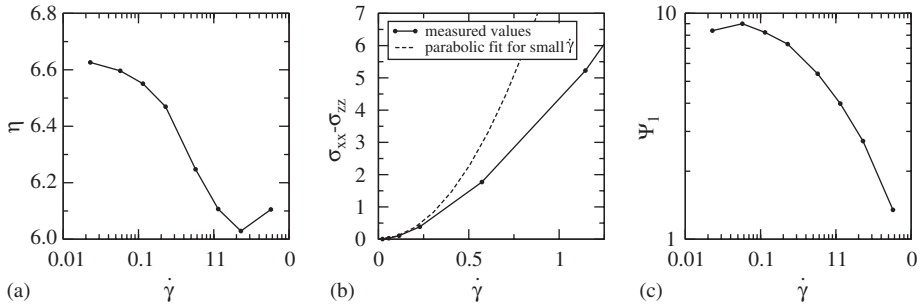

Fig. 2. (a) Viscosity as a function of the shear rate. For large shear rates the viscosity decreases slightly (shear thinning). (b) First normal stress difference and (c) first normal stress coefficient. The normal stress difference is quadratic for small shear rate $\dot{\gamma}$, but the coefficient decreases significantly for $\dot{\gamma} \gtrsim 1$.

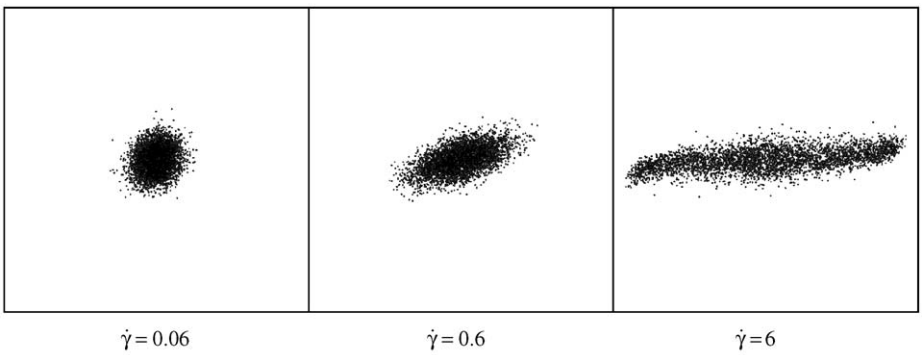

Fig. 3. Distribution of dumbbell configurations in the shear plane. Each dot corresponds to the end-to-end vector of a dumbbell in the xz plane. For small $\dot{\gamma}$ the orientation is isotropic, at moderate shear rates it is an elongated ellipse, and at large shear rates it is further deformed. The sides of the box represent the maximum elongation $r_{\max}$ of the FENE springs.

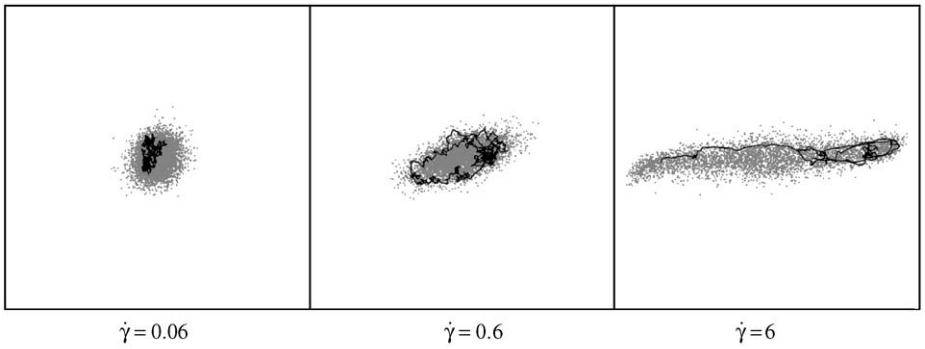

Fig. 4. Trajectories of the configuration of a dumbbell at different shear rates. A selected dumbbell is traced for 50 time units for the two smaller shear rates, and 20 time units for the largest shear rate.

the dumbbells can relax. This is augmented with the rotational component of the shear flow to yield a tumbling motion.

4. Summary

In conclusion, we presented preliminary results on extending DPD for viscoelastic fluids by connecting DPD particles to form dumbbells. The model shows (shear rate dependent) normal stress difference, and a small amount of shear thinning. This is our first step to study numerically the instabilities and turbulence in viscoelastic fluids with a method complementary to direct numerical simulations of the constitutive equations. To fully establish our model, in future work we will make quantitative comparisons to analytical and numerical results of other models.

Acknowledgements

This research has been supported by the PHYNECS training network of the European Commission under contract HPRN-CT-2002-00312. We thank Mar Serrano for useful discussions.

References

[1] R.G. Larson, Constitutive Equations for Polymer Melts and Solutions, Butterworth, Stoneham, MA, 1988.
[2] R.B. Bird, R.C. Armstrong, O. Hassager, Dynamics of Polymeric Liquids, vol. 1, Fluid Mechanics, Wiley, New York, 1987.
[3] B. Meulenbroek, C. Storm, V. Bertola, C. Wagner, D. Bonn, W. van Saarloos, Intrinsic route to melt fracture in polymer extrusion: a weakly nonlinear subcritical instability of viscoelastic Poiseuille flow, Phys. Rev. Lett. 90 (2003) 024502.
[4] B. Meulenbroek, C. Storm, A.N. Morozov, W. van Saarloos, Weakly nonlinear subcritical instability of visco-elastic Poiseuille flow, J. Non-Newtonian Fluid Mech. 116 (2004) 235–268.
[5] R.G. Larson, Fluid dynamics: turbulence without inertia, Nature 405 (2000) 27–28.
[6] A. Groisman, V. Steinberg, Elastic turbulence in a polymer solution flow, Nature 405 (2000) 53–55.
[7] R.G. Owens, T.N. Phillips, Computational Rheology, Imperial College Press, London, 2002.
[8] P.J. Hoogerbrugge, J.M.V.A. Koelman, Simulating microscopic hydrodynamic phenomena with dissipative particle dynamics, Europhys. Lett. 19 (1992) 155–160.
[9] P. Espanol, P. Warren, Statistical-mechanics of dissipative particle dynamics, Europhys. Lett. 30 (1995) 191–196.
[10] S. Chen, N. Phan-Thien, X.-J. Fanc, B.C. Khoo, Dissipative particle dynamics simulation of polymer drops in a periodic shear flow, J. Non-Newtonian Fluid Mech. 118 (2004) 65–81.
[11] R.D. Groot, P.B. Warren, Dissipative particle dynamics: bridging the gap between atomistic and mesoscopic simulation, J. Chem. Phys. 107 (1997) 4423–4435.
[12] I. Goldhirsch, C. Goldenberg, On the microscopic foundations of elasticity, Eur. Phys. J. E 9 (2002) 245–251.